

Early-age thermal analysis and strain monitoring of massive concrete structures

Yan Geng^{1a}, Xiongyan Li^{*1}, Suduo Xue^{1b}, Jinguang Li² and Yanjie Song²

¹College of Architecture and Civil Engineering, Beijing University of Technology,
No.100, Pingleyuan, Chaoyang District, Beijing 100124, China

²Department of Civil Engineering, China Huanqiu Contracting & Engineering Co. Ltd.,
No.1, Chuangda 2nd Road, Chaoyang District, Beijing 100012, China

(Received September 15, 2017, Revised November 15, 2017, Accepted December 14, 2017)

Abstract. Hydration heat and thermal induced cracking have always been a fatal problem for massive concrete structures. In order to study a massive reinforced concrete wall of a storage tank for liquefied natural gas (LNG) during its construction, two mock-ups of 0.8 m×0.8 m×0.8 m without and with metal corrugated pipes were designed based on the actual wall construction plan. Temperature distribution and strain development of both mock-ups were measured and compared inside and on the surface of them. Meanwhile, time-dependent thermal and mechanical properties of the concrete were tested standardly and introduced into the finite-element (FE) software with a proposed hydration degree model. According to the comparison results, the FE simulation of temperature field agreed well with the measured data. Besides, the maximum temperature rise was slightly higher and the shrinkage was generally larger in the mock-up without pipes, indicating that corrugated pipes could reduce concrete temperature and decrease shrinkage of surrounding concrete. In addition, the cooling rate decreased approximately linearly with the reduction of heat transfer coefficient h , implying that a target cooling curve can be achieved by calculating a desired coefficient h . Moreover, the maximum cooling rate did not necessarily decrease with the extension of demoulding time. It is better to remove the formwork at least after 116 hours after concrete casting, which promises lower risk of thermal cracking of early-age concrete.

Keywords: hydration degree; time-dependent thermal property; thermal analysis; finite-element simulation; LNG storage tank; reinforced concrete; strain monitoring

1. Introduction

Reinforced concrete (RC) is usually utilized to construct the outer wall of LNG storage tanks for its good resistance to cryogenic temperatures, buckling, fire and earthquake (Jeon *et al.* 2007, Dahmani 2011). For the consideration of bearing capacity, durability and storage safety, large dimensions of concrete structural components are usually utilized during construction, with the minimum size of 0.8 m for walls, 1.0 m for platforms and 1.2 m for counterfort columns. Therefore, it is of great significance to study the problems of simulating and controlling hydration heat of massive concrete (Zhu 2013, Wang *et al.* 2013) and the heat induced cracking (Klemczak 2014, Buffo-LacARRIERE *et al.* 2011) which is fatal for the durability and impermeability of LNG storage tanks.

Many experimental and analytical studies have been conducted to investigate thermal distribution and stress of massive concrete structures (Amin *et al.* 2009, ACI 231

2010). Zhou *et al.* (2014) simulated the temperature and strain distribution in a subway station structure with their proposed hydration degree evaluating equation and the finite element (FE) program developed for hydration heat analysis, of which the simulation results agreed well with the site-measured data. Their study also indicated that creep doesn't always reduce the undesirable tensile stress. Wang *et al.* (2016) carried out a construction simulation of reinforced concrete bridge piers for a heat transfer problem as well as a thermal stress problem and concluded that a high initial concrete temperature could result in a high extreme internal temperature, which caused the early peak temperature and the larger principle stresses. Qin *et al.* (2014) developed the equivalent age-hydration degree curve and accurately simulated the hydration temperature field in the slab of Taishan nuclear power plant unit 2, considering effects of age, temperature and construction process on hydration thermal field of concrete. What's more, some researchers also took the effect of humidity into consideration when simulating thermal field and strain development of concrete. Di Luzio and Cusatis (2009) developed a new hygro-thermo-chemical model for high-performance concrete suitable for the analysis of moisture transport and heat transfer at the early age and beyond. The proposed model simulated early age phenomena with great accuracy by comparison with experimental test data (Di Luzio and Cusatis 2009). Jendele *et al.* (2013) formulated a

*Corresponding author, Associate Professor

E-mail: xiongy2006@126.com

^aProfessor

E-mail: sdxue@bjut.edu.cn

^bPh.D. Student

E-mail: gengyan11@163.com

multi-scale analysis accounting for a high variety of cement properties, concrete composition, structure geometry and boundary conditions. The validation on selected structures showed a good prediction of temperature fields during concrete hardening and a reasonable performance of the mechanical part. Nevertheless, only some of the researches implemented standard tests to obtain the time-varying thermal and mechanical properties of the certain concrete at early age. Zreiki *et al.* (2010) developed a thermo-chemo-mechanical model on the basis of complete material characterization experiments to predict the early-age development of strains and residual stresses and the coupled model showed good capability to predict the risk of cracking. Besides, only a few studies focused on the outer wall of LNG storage tank during construction period. Zhai *et al.* (2016) studied the temperature and thermal stress distribution on the concrete wall of a 160,000 m³ LNG tank by the FE method and found that the cracks in vertical direction appeared at the concrete wall surface and the cracks in circumferential direction appeared at the buttress column surface.

For the hydration heat model of concrete, many forms of hydration degree theory have been proposed in previous studies. De Schutter (2002) developed a simulation procedure based on the degree of hydration as a fundamental parameter, which is related with the microstructural development during cement hydration. Accurate finite element simulations were obtained for the problem of early age thermal cracking. Besides, Anka Ilc *et al.* (2009) presented a new numerical model for the prediction of temperature development in young concrete structures with experimental adiabatic hydration curves and an artificial neural networks approach. Although some researchers have considered the influence of reinforcement on temperature field and thermal stress in construction (Chen 2006), few studies discussed the influence of corrugated pipes embedded in the concrete, which can serve as a cooling approach for temperature controlling in practice of future research and engineering projects.

In this study, a simplified hydration degree function was proposed based on standard hyperbolic hydration model, readjusted with the tested concrete adiabatic temperature rise curve. Two cubic RC mock-ups with the dimensions 0.8 m×0.8 m×0.8 m were cast simultaneously on two RC bases of 1.1 m×1.1 m×0.2 m in the laboratory using the designed concrete mix proportion and reinforcement of an actual LNG storage tank project to be constructed in China. One of them was arranged corrugated pipes in the middle according to the practical construction design. The influence of the pipes on temperature field and strain distribution was analyzed by comparing the temperature and strain results obtained from the PT100 temperature sensors and vibration wire sensors in the mock-ups. In addition, redevelopment was employed to refine the subroutine utilized in the FE software and time-varying thermal and mechanical properties were adopted in the simulation, which were based on the previously conducted standard experiments. Moreover, parametric analysis of the influence of heat transfer coefficient and demoulding time on the cooling rate was conducted to discuss the approach to achieve a target cooling curve and the suitable

demoulding time in future projects. It is promising that research findings of this paper can be applied to not only the outer wall of LNG storage tanks but also other massive concrete structures with similar reinforcement and corrugated pipes.

2. Model of heat transfer

Temperature distribution in adiabatic concrete blocks can be calculated by the three dimensional transient heat conduction equation (Abbasi and Hogg 2005) as shown in Eq. (1)

$$c\rho \frac{\partial T}{\partial t} = \lambda \left(\frac{\partial^2 T}{\partial x^2} + \frac{\partial^2 T}{\partial y^2} + \frac{\partial^2 T}{\partial z^2} \right) + \frac{dQ(t)}{dt} \quad (1)$$

where ρ is the concrete density (in kg/m³), c is the concrete specific heat (in J/(kg·°C)), t is time variable since casting of concrete (in second), λ is the concrete thermal conductivity (in W/(m·°C)), $dQ(t)/dt$ is the rate of internally generated heat with time t (in W/m³), $Q(t)$ is cumulative heat of hydration per unit mass of concrete with time t (in J/g).

For a standard hyperbolic hydration model, adiabatic temperature rise can be calculated by Eq. (2) (Cai 1979)

$$Q(t) = Q_{\infty} \frac{t}{M+t} \quad (2)$$

where Q_{∞} is the cumulative heat of hydration per unit mass of concrete at complete hydration (in J/g), M is a parameter which theoretically equals to the time t_h when the concrete reaches half of the complete hydration.

However, the adiabatic temperature rise calculated through this model does not allow for the influence of hydration rate. Although some researchers suggested replacing time variable t with equivalent age t_e according to Arrhenius based equation (Hattel and Thorborg 2003), the value of activity energy of the binder is always empirical (ASTM C1074-11 2011). Therefore, a new hyperbolic model which is readjusted with hydration degree $\alpha(t)$ is proposed and defined as the ratio of cumulative hydration heat of reacted binder to the cumulative hydration heat at complete hydration and ranges from 0 to 1, as given in Eq. (3)

$$\alpha(t) = \frac{Q(t)}{Q_{\infty}} = \frac{t}{m(t)+t} \quad (3)$$

where $m(t)$ replaces the constant parameter M in Eq. (2) and varies with time t . It is inversely related to the tested adiabatic hydration rate, as Eq. (4)

$$m(t) = a - b \frac{dT(t)}{dt} \quad (4)$$

where a and b are regression parameters calculated through nonlinear fitting and $m(t_h)=t_h$.

Since $\alpha(t)$ should be monotonically increasing according to its definition, any declination during computation, if occurring, will be reset to the highest value previously calculated.

Besides confirming the model for hydration heat, boundary and initial conditions are also required to solve the heat conduction equation. All heat reaching the boundary surface is released by convection conforming to the third type of boundary condition (Asan 2006). Since the concrete element is assumed to be isotropic, the heat convective flux equation is expressed as

$$\lambda \frac{\partial T}{\partial n} = h(T_e - T_c) \quad (5)$$

where n refers to any coordinate axis among x , y and z , T_e is environmental temperature (in °C), T_c is concrete surface temperature (in °C), h is surface heat transfer coefficient (in $W/(m^2 \cdot ^\circ C)$). The surface heat transfer coefficient h is closely related to physical properties and flow velocity of the fluid surrounding the structure, shape and area of the contact surface and so forth. A higher value of h implies more intensive heat exchange between concrete and surrounding environment. In this paper, h of the two cubic RC mock-ups differs before and after demoulding. As for Mock-up B, h also differs around the pipes and the concrete surface.

Since all the factors in Eq. (1)-Eq. (5) have been determined, redevelopment of FE subroutine by Fortran can be carried out to define user-defined material property (including heat generation rate in Eq. (1), hydration degree in Eqs. (3) and (4) and relative parameters in Subroutine UMATHHT) and boundary conditions (in Subroutine FILM) to accomplish the FE simulation in ABAQUS.

3. Experiments and simulation

3.1 Material property tests

Since it is a preliminary study of an actual LNG construction project, the designed concrete mix proportion of the project was adopted. As listed in Table 1, this study used ordinary Portland cements with the grade of 42.5 containing ground granulated blast furnace slag complying with the Chinese National Standard GB175 (2015), crushed limestone of 5-20 mm in size, natural river sand with medium size and polycarboxylate superplasticiser. The compressive strength of concrete was tested according to GB/T 50081 (2002) and the 28-day compressive strength was 62.1 MPa. The water-binder ratio was 0.31.

The adiabatic temperature rise curve of the concrete was measured using a BY-ATC/JR concrete adiabatic temperature measuring instrument with an accuracy of 0.02°C developed by Building Materials Research Institute

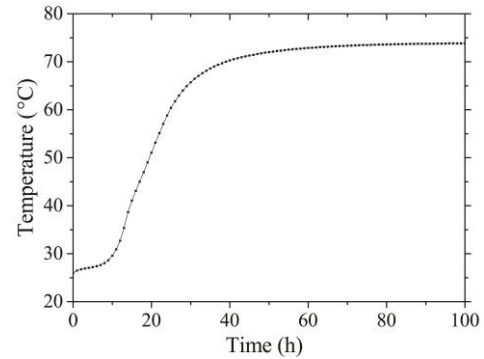


Fig. 1 Adiabatic temperature rise curve

of Tsinghua University. The adiabatic temperature rise is 47.85°C within the first 100 hours(h) in the condition that the casting temperature is 26.01°C and the tested curve is shown in Fig. 1. With this adiabatic temperature rise curve, the parameters a and b in Eq. (4) was calculated as 26.8 and 5.2 respectively and therefore $\alpha(t)$ was derived.

In most analysis about temperature field within concrete structures (Martinelli *et al.* 2013) at early age, thermal parameters are based on empirical values. However, in this study, λ and c were obtained from concrete thermal conductivity tests according to GB/T 10294 (2008) and specific heat tests according to SL 352 (2006) respectively.

Totally thirteen sets of casting ages, namely 1day(d), 2d, 3d, 5d, 7d, 10d, 14d, 20d, 28d, 45d, 60d, 90d and 120d, were chosen considering the individual variation of concrete with the specific mix proportion and the time-dependent variation with casting ages. The experiment results of λ and c are shown in Fig. 2 and Fig. 3.

In general, the values of c stay within the range of empirical value, while the values of λ deserve more discussion. As is known, thermal conductivity of concrete is greatly affected by mix proportioning, aggregate types and sources, as well as moisture status and unit weight in the dry state (Nevile 1995). ACI Committee 207 (2007) recommends the range of λ between 1.9-3.3 $W/(m \cdot ^\circ C)$ in accordance with different aggregates for normal concrete temperature and high moisture at early age, however Jendele (2014) illustrates that the recommended value is 1.5 $W/(m \cdot ^\circ C)$ for dry concrete and 1.7 $W/(m \cdot ^\circ C)$ for water-saturated concrete in the Czech ČSN 731208 standard. (According to Kim 2003), thermal conductivity dramatically decreases as the moisture status changes from fully saturated to fully dried and replacement of cement by fly ash or slag makes the coefficient drop. Therefore, considering the component of slag in the concrete proportion and relative humidity conditions of the test samples, the values of λ presented in this paper are acceptable.

In addition, it was also found that the values of λ and c both varied relatively greatly during the first 7days, which may resulted from the change of hydration degree and different amount of reaction products during hydration process. Therefore, the test values of λ and c in the first 7 days were directly written into the heat generation subroutine in FE software. After the first 7 days, λ remained nearly the same and was set as a constant of 1.54 $W/(m \cdot ^\circ C)$

Table 1 Mix proportion of concrete

Material	Type	Proportion (kg/m^3)
Cement	P.O 42.5	310
Slag powder	S95	142
Water	Tap water	140
Fine aggregate	Medium river sand	759
Coarse aggregate	Crushed stone 5~20 mm	1006
Superplasticiser	FAC	9.04

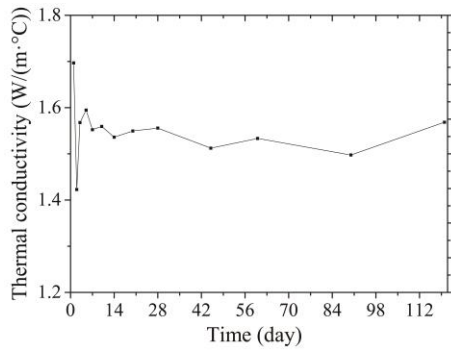


Fig. 2 Thermal conductivity curve

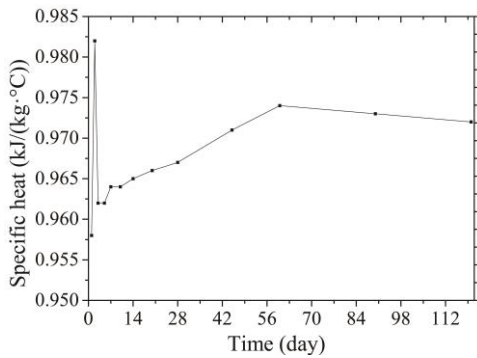


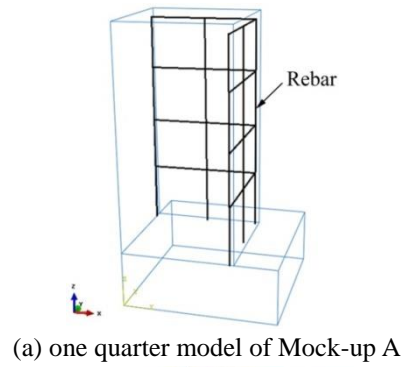
Fig. 3 Specific heat curve

in the subroutine, while c linearly increased up to 60days and finally reached a constant of $0.974 \text{ kJ}/(\text{kg}\cdot^{\circ}\text{C})$.

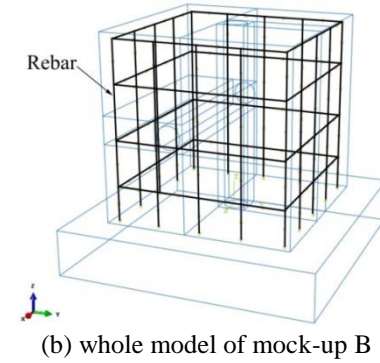
3.2 Mock-up description

In order to study the temperature and strain distribution, two RC mock-ups with the dimensions $0.8 \text{ m}\times 0.8 \text{ m}\times 0.8 \text{ m}$ were constructed using the concrete mentioned above and were reinforced as shown in Fig. 4. A RC base with the dimensions $1.1 \text{ m}\times 1.1 \text{ m}\times 0.2 \text{ m}$ was also constructed in advance for each mock-up to provide a fixed constraint and temperature boundary similar to practical conditions. As the mock-ups were designed based on of a LNG storage tank project, both the reinforcement of rebars and arrangement of corrugated pipes (through which pre-stressed steel will be installed after the concrete are mature in actual construction) resembled the actual wall construction plan. The concrete block without corrugated pipes was named as Mock-up A and the one with pipes was named as Mock-up B for contrast. The 18 mm thick plywood (offered by Langfang Dadi Wood Co. Ltd.) with conductivity of $0.15 \text{ W}/(\text{m}\cdot^{\circ}\text{C})$ was used for both mock-ups and removed from the concrete mock-up at 44h after casting. After demoulding, both mock-ups were exposed to the same laboratory environment.

In the FE model, 8-node linear heat transfer solid elements (DC3D8) were used for concrete and 2-node heat transfer truss elements (DC1D2) were used for steel rebars. In the FE software ABAQUS, ambient temperature T_e and heat convection coefficient h are two important factors when simulating the temperature field in the concrete. There were generally four kinds of surfaces in this model,

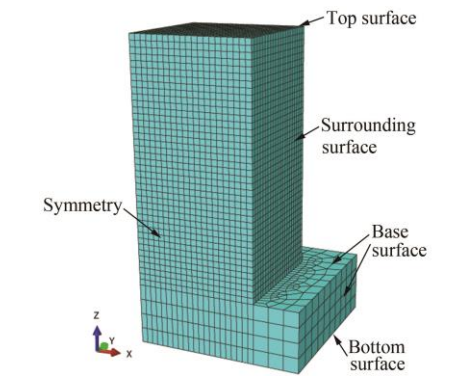


(a) one quarter model of Mock-up A

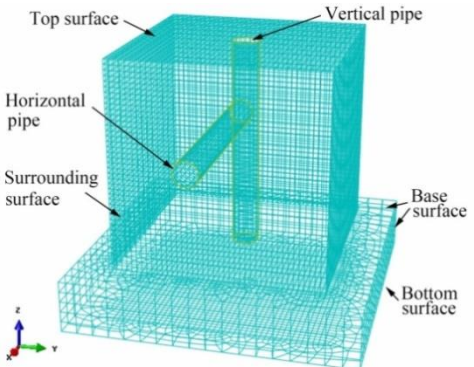


(b) whole model of mock-up B

Fig. 4 The reinforcement of two mock-ups



(a) one quarter model of Mock-up A



(b) whole model of mock-up B

Fig. 5 The Finite-element models and surface names of the two mock-ups

namely top surface, surrounding surface, base surface and bottom surface. For mock-up B, there were two more surfaces along the vertical and horizontal pipes. The Finite-element models and surface names of the two mock-ups are

Table 2 Boundary conditions of the two mock-ups

Boundary condition	Location	Value	
Heat convection coefficient h [W/(m ² ·°C)]	top and base surface	9.0	
	surrounding surface (Before demoulding)	4.5	
		9.0	
	surrounding surface (After demoulding)	Bottom surface	3
		horizontal pipe surface	2.5
vertical pipe surface	2.5		
Initial temperature(°C)	Upper cube	8.54	
	Lower base	15.9	

shown in Fig. 5. Since mock-up A is symmetric in both x and y direction, only one quarter model was established.

It should be noted that heat convection coefficient of surrounding surfaces varies before and after the timber demoulding, which is an important factor influencing the cooling of concrete cubes. The values of heat convection coefficient around different surfaces are listed in Table 2. The value of h for top and base surface was assumed to be 9.0 W/(m²·°C), slightly higher than 8.7 W/(m²·°C) for the inner wall recommended by GB 50176(2016), since the lab room was very close to the entrance door which may occasionally accelerate air flow and intensify convection in the lab. The value of h for surrounding surfaces before demoulding and the value for bottom surface was calculated through the heat-resistance method (GB 50176) and heat transfer coefficient calculation equation (GB 50736). Overall, the values of h in Table 2 were very close to the results reported by Lee *et al.* (2009).

3.3 Sensor arrangement

Totally twenty PT100 temperature sensors (numbered from 1 to 20) and ten BGK 4200 vibration wire (VW) strain sensors (numbered from V1 to V10) were tightly tied up to rebars with iron wire at the specified position. Polyethylene formed plastic patches were used to fill up the space between the VW sensor and the rebar to keep the sensor straight and make the binding more secure. Six foil strain gauges (numbered from S1 to S6) were effectively pasted to the surface of the concrete immediately after the formwork was removed. The arrangement of all the sensors is shown in Fig. 6. Generally, three layers of sensors were arranged in the cube from the bottom to the top. Every monitoring point in Mock-up B had a corresponding sensor in Mock-up A and both share the same coordinates. Since the middle cross section was theoretically calculated to reach the highest temperature, eight temperature sensors in Mock-up A and seven temperature sensors in Mock-up B were intensively arranged along both the diagonal direction and center lines.

Besides, two temperature sensors were installed at the bottom and top layer respectively in each mock-up. As for VW sensors, they were all arranged along x axis, with two at the bottom layer, two at the middle layer and one at the top layer. The numbered foil strain gauges were all pasted horizontally along the central line of the surface. The sensors installed in the concrete are shown in Fig. 7. Since the ambient temperature changed over time, one PT100 sensor was arranged to collect the environment temperature data and another was embedded in the lower concrete base, the data of which were utilized in FE analysis to make the boundary condition more consistent with actual situation.

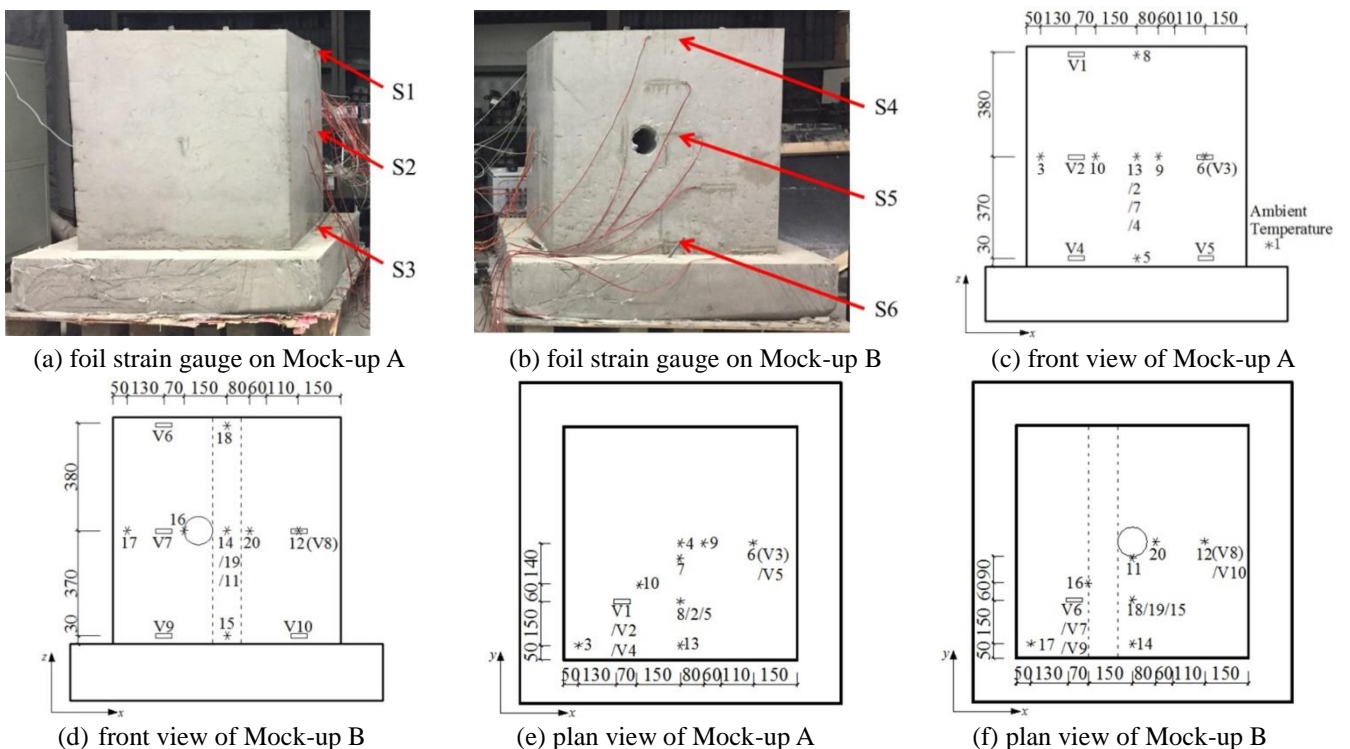


Fig. 6 Sensors arrangement in the two mock-ups



Fig. 7 Sensors tied to the rebars and pipes

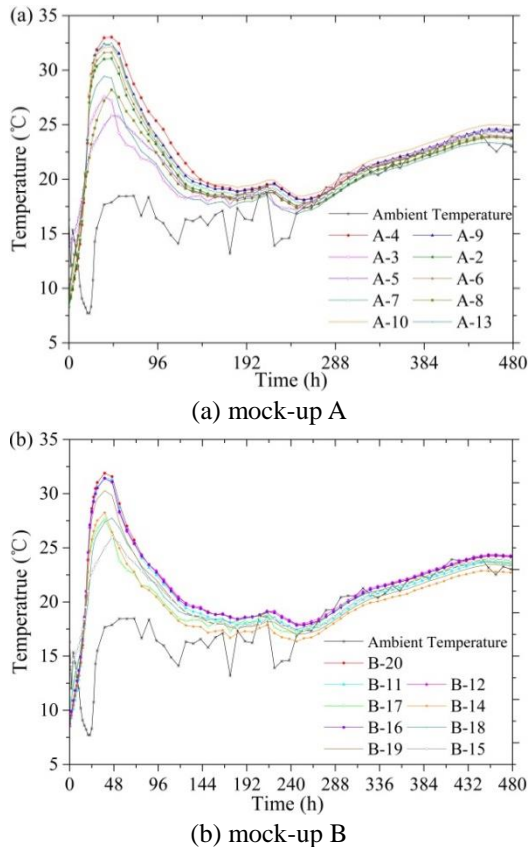


Fig. 8 Tested curves of the PT100 sensors in the concrete cube

4. Results and discussion

4.1 Temperature comparison

4.1.1 Comparison between Mock-up A and B

Thirty days of temperature data in the two mock-ups were measured every half an hour immediately after casting. As shown in Fig. 8, temperature within both mock-ups increased rapidly during the first 28 hours and the core part remained a highest temperature stage up to 60h.

The highest temperature in Mock-up A and B was 33.03°C at 44h and 31.95°C at 40h respectively. The maximum temperature rise in Mock-up A and B were 24.49°C and 23.41°C respectively. Then, temperature began to decrease gradually and the cooling stage lasted up to around 180h. The maximum temperature decline per hour

in Mock-up A and B was $0.29^{\circ}\text{C}/\text{h}$ and $0.36^{\circ}\text{C}/\text{h}$. Afterwards, the temperature within the concrete attained ultimately stable from inside to outside, only fluctuating with environment temperature. This stage was named as the stable stage. Although the overall temperature trends of Mock-up A and B were similar, behaviors on the cooling stage still showed slight difference. The temperature descending of mock-up B after demoulding was relatively sharper than that of Mock-up A, which indicated that demoulding may have greater influences on the mock-up with corrugated pipes.

To discuss the influence of pipes on temperature distribution in detail, representative monitoring points with the same coordinates, namely Sensor 2, 3, 5, 7, 10, 13 in Mock-up A and the corresponding Sensor 19, 17, 15, 11, 16, 14 in Mock-up B were compared respectively and the results are shown in Fig. 9. The sensor numbers are prefixed with letter A and B respectively, for example A-2 and B-19. It was noticed that the temperature of monitoring points near the pipes were marginally influenced by heat convection between pipes and the inner air. The maximum differences at the highest temperature stage between A-7 and B-11, A-10 and B-16, A-2 and B-19, A-13 and B-14 were 0.99°C , 0.91°C , 0.82°C and 1.20°C respectively, while the maximum differences at the cooling stage were 2.56°C , 2.67°C , 2.34°C and 2.84°C respectively, as shown in (a), (c), (d) and (f) in Fig. 9. Nevertheless, the temperature curves of the points far from the pipes showed little difference, such as A-3 and B-17.

4.1.2 Comparison between test data and FE analysis

Apart from laboratory testing data, FE analysis results with a time increment of 2 hours were also obtained to validate the proposed hydration model. The comparing results of representative points in Mock-up A, namely Point 4 in the center, Point 3 at the edge of middle layer, Point 8 at the top layer and Point 5 at the bottom layer, are shown in Fig. 10.

All these four testing points manifested similar trends between the measured data and calculated results. The maximum differences of peak values of rising temperature were 0.01°C , 0.84°C , 0.09°C and 0.88°C respectively, as shown from (a) to (d) in Fig.10, demonstrating that the proposed hydration model can effectively capture the highest temperature point. Though the maximum differences of peak values of Point 3 and 5 were much larger than those of Point 4 and 8, the average differences throughout the monitoring duration were quite similar, with the value of 0.36°C , 0.32°C , 0.17°C , 0.18°C respectively from (a) to (d) in Fig. 10. Despite the significant resemblance between the measured and calculated curves on the whole, the standard deviations throughout the monitoring duration were 3.10°C , 1.66°C , 1.89°C and 1.61°C respectively from (a) to (d) in Fig. 10. It indicates that some deviations still exist in the FE analysis, especially at the rapidly ascending stage and at the first hours of the stable stage. For example, the difference between the measured and calculated curve of Point 5 may be caused by the simplification of bottom boundary condition in the simulation. In addition, the difference between the measured and calculated curves of Point 4 and Point 3 at the

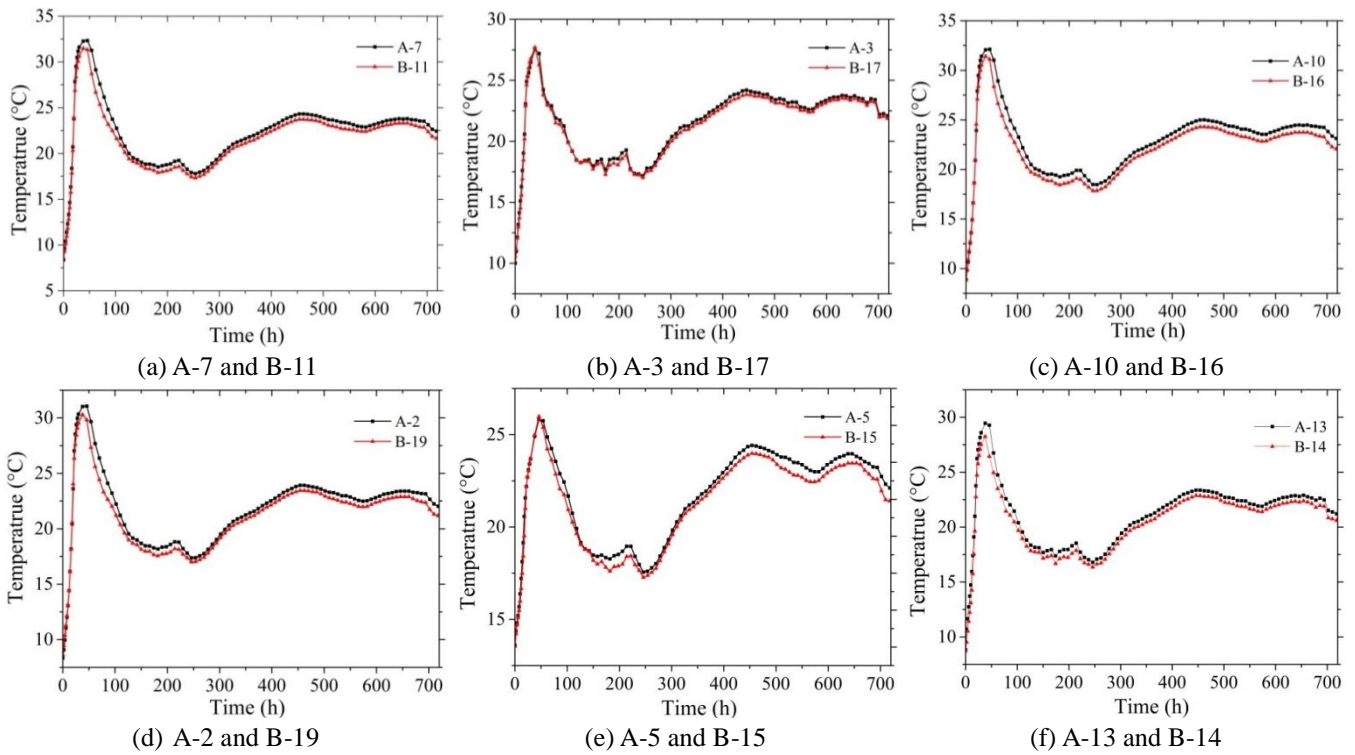


Fig. 9 Measured curves of Mock-up A and B at representative monitoring points

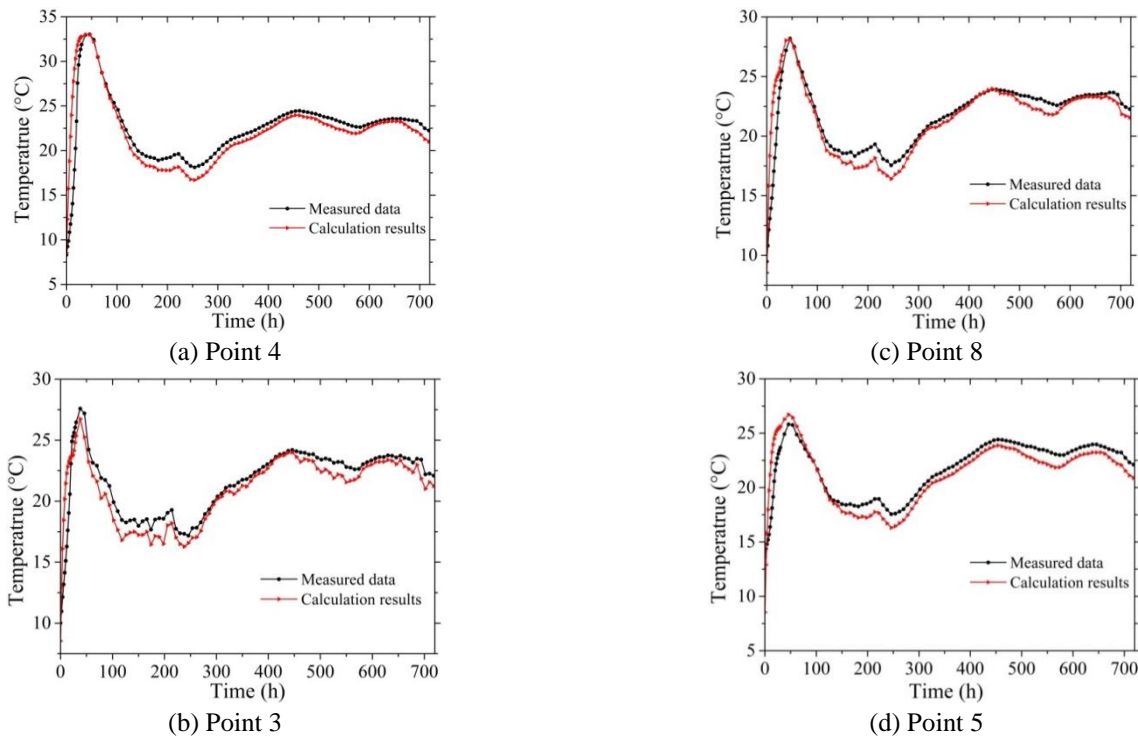


Fig. 10 Measured data and calculation results of Mock-up A at representative points

Fig. 10 Continued

cooling stage may result from the fluctuation of environment airflow, hence influencing the value of heat transfer coefficient h .

4.1.3 The influence of curing approaches

The cooling rate of concrete after demoulding is directly

influenced by curing approaches. Different curing approaches lead to different values of heat transfer coefficient h . Since the measured curves differed a little from the calculated ones at the cooling stage and the beginning of the stable stage, totally four sets of FE analysis on the condition of different values of h after demoulding for Mock-up A were studied to discuss the influence of h on

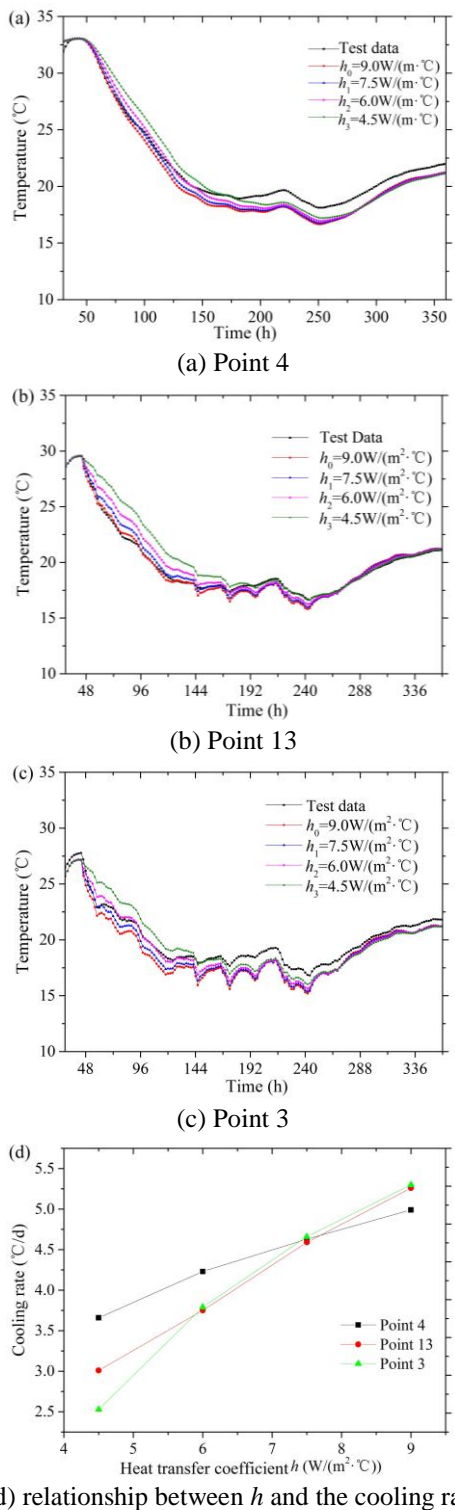


Fig. 11 Calculated temperature curves with different values of h at representative points

temperature decrease of the concrete, namely $h_0=9W/(m^2 \cdot ^\circ C)$, $h_1=7.5W/(m^2 \cdot ^\circ C)$, $h_2=6W/(m^2 \cdot ^\circ C)$ and $h_3=4.5W/(m^2 \cdot ^\circ C)$. The condition of h_0 referred to the condition exposed to lab environment without a curing cover and the conditions of $h_1 \sim h_3$ could correspond to different thickness of curing blanks or different materials of curing covers.

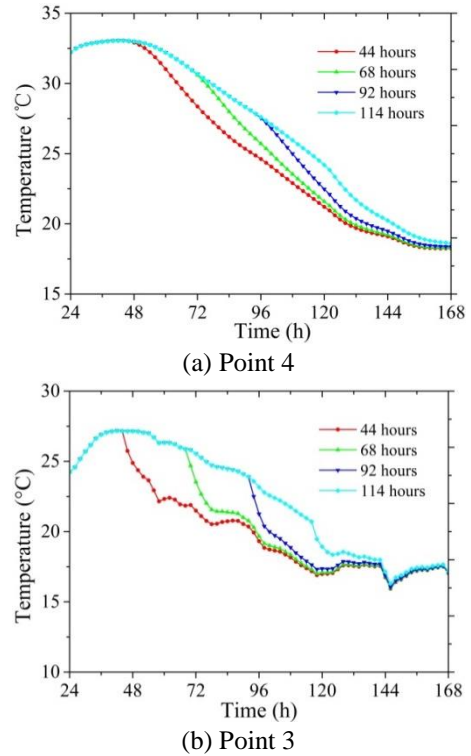


Fig. 12 Calculated temperature curves of representative points with different demoulding time

The comparing curves of representative points were shown in Fig. 11, namely Point 4 in the center, Point 13 near the edge and Point 3 in the corner. Generally, heat transfer coefficient h mainly influenced the cooling rate of concrete, whereas making little difference to the highest temperature and the stationary temperature it reached. The maximum cooling rates per day of Point 4 were $4.99^\circ C/d$, $4.63^\circ C/d$, $4.23^\circ C/d$ and $3.66^\circ C/d$ respectively on the conditions from h_0 to h_3 . In the same way, the maximum cooling rates per day of Point 13 were $5.26^\circ C/d$, $4.59^\circ C/d$, $3.75^\circ C/d$ and $3.01^\circ C/d$ respectively and those of Point 3 were $5.30^\circ C/d$, $4.66^\circ C/d$, $3.79^\circ C/d$ and $2.53^\circ C/d$ respectively. It was noticed that the points in the corner were most sensitive to the variation of h . Moreover, the cooling rate decreased approximately linearly with the reduction of h , as shown in Fig.11 (d). It implies that a target cooling curve can be achieved by calculating a desired cooling rate and its corresponding heat transfer coefficient h , thereby selecting appropriate concrete curing approaches and effectively controlling the cooling stage as needed.

4.1.4 The influence of demoulding time

Demoulding time is an important factor in construction, since it usually saves time and cost and accelerates construction process if the formworks are removed earlier. However, inappropriate demoulding time indicates that the concrete structures are more easily influenced by ambient environment such as temperature, humidity, air flow and so forth, which is fatal to temperature gradient and crack evolution inside concrete. To further learn the influence of demoulding time on cooling rate, totally four sets of FE

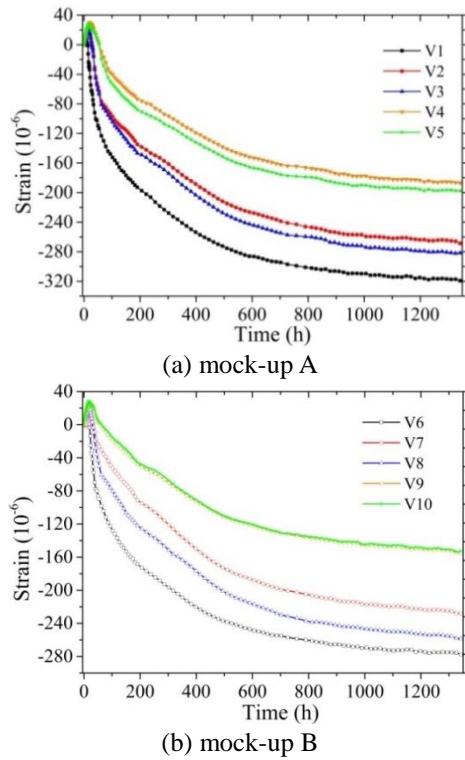


Fig. 13 Strains in the concrete acquired from VW sensors

analysis on the condition of demoulding time at $t_0=44\text{h}$, $t_1=68\text{h}$, $t_2=92\text{h}$ and $t_3=116\text{h}$ were carried out. The calculated temperature curves of Point 4 in the center and Point 3 in the corner were compared as shown in Fig. 12. The maximum cooling rates per day at Point 4 were 4.99°C/d , 5.61°C/d , 5.14°C/d and 4.28°C/d respectively, and the maximum cooling rates per day at Point 3 were 5.30°C/d , 5.09°C/d , 6.26°C/d and 4.24°C/d respectively on the four conditions from t_0 to t_3 . It was noticed that the maximum cooling rate per day did not necessarily decrease with the extension of demoulding time from 44h to 92h. It indicates that it is better to remove the formwork at least after 116 hours after concrete casting, which promises lower risk of thermal cracking of concrete.

4.2 Strain monitoring

VW strain sensors and foil strain gauges were used to monitor the strain variations in the concrete and at the surface respectively. Strain variation curves of 60 days in the concrete acquired from VW sensors are shown in Fig. 13, where positive strain indicates expansion of concrete while negative strain indicates shrinkage. As Fig. 13 shows, the strain of inner concrete promptly increased due to temperature rise caused by hydration heat. After the intense hydration reactions, the strain began to flop because of autogenous shrinkage, drying shrinkage and thermal contraction till the overall shrinkage gradually arrived at a relatively stable stage and decreased moderately.

It was noticed that the contraction in the upper layer was obviously larger than the lower layer for both mock-ups and the largest contraction values measured in Mock-up A and Mock-up B were 319×10^{-6} and 278×10^{-6} . Moreover, the

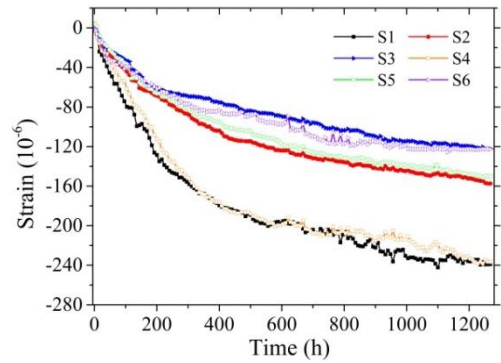


Fig. 14 Surface strain curves

strain decrease of the upper layer was far more rapid than that of the lower layer at the flopping stage. However, the maximum positive strain occurred in the lower layer and the values measured in Mock-up A and B were 29×10^{-6} at 21h and 28×10^{-6} at 19h after initial setting respectively. After all, both expansion and contraction strains were relatively small for the concrete material used in this experiment, indicating that the risk of cracking in the concrete was also small. Meanwhile, the contraction in Mock-up A was generally larger than that in Mock-up B, which may be due to the existence of corrugated pipes. On one hand, corrugated pipes reduced the consumption of concrete. On the other hand, the existence of pipes marginally decreased the temperature difference between inner concrete and ambient environment.

As for the surface strain, since the foil strain gauges were pasted to the mock-up surface after the formwork was removed and the overall temperature of the mock-ups began to decrease, there were few positive strains during measurement and the maximum contraction strains on the surface of Mock-up A and B were 239×10^{-6} and 238×10^{-6} respectively. The surface strain curves (as shown in Fig. 14) fluctuated within a range of $\pm 5\%$, which may resulted from the fluctuation of environment temperature, the precision of the static data acquisition instrument and the pasting quality of the foil gauges. Overall, there were no visible cracking on all the surfaces of both mock-ups.

Prospectively, since the existence of corrugated pipes could reduce the concrete temperature around the pipe and decrease the contraction of inner concrete, those corrugated pipes may be possible for utilizing as part of an air cooling approach in controlling the temperature rise in the concrete and lowering the risk of thermal induced cracking. However, more detailed investigation should be undertaken for this air cooling approach to establish an accurate and effective relationship between in-pipe heat convection coefficient and air speed to thoroughly grasp the cooling discipline and develop an integrated temperature and cracking control system.

5. Conclusions

A simplified hydration degree function was proposed based on standard hyperbolic hydration model and readjustment with the tested concrete adiabatic temperature

rise curve in this paper. Two cubic reinforced concrete mock-ups of 0.8 m×0.8 m×0.8 m with and without metal corrugated pipes were cast to measure and compare the temperature distribution and strain development in the concrete and on the surface. The primary conclusions are drawn as follows:

- A new type of hydration degree model was proposed based on standard hyperbolic hydration model and readjustment with the tested concrete adiabatic temperature rise curve. A FE simulation subroutine was developed to calculate the temperature field in the concrete mock-ups. The calculation results agreed well with the measured data, validating the effectiveness of the proposed hydration degree model.
- The cooling rate of concrete decreased approximately linearly with the reduction of heat transfer coefficient h , which implies that a target cooling curve can be achieved by calculating a desired cooling rate and its corresponding heat transfer coefficient h , thereby effectively controlling the cooling stage as needed.
- The contraction in the upper layer was obviously larger than the lower layer, which should be given more consideration in cracking control. However, the maximum positive strain occurred in the lower layer. After all, both expansion and contraction strains were relatively small for the concrete material used in this experiment, indicating that the risk of cracking in the concrete was very small.
- The maximum temperature rise was slightly higher and the contraction was marginally larger in Mock-up A than that in Mock-up B, indicating that the existence of corrugated pipes can reduce the concrete temperature surrounding the pipe and decrease the contraction of concrete.

Acknowledgments

This research is financially supported by China Huanqiu Contracting & Engineering Co. Ltd. under grant number 2015GJTC-07-01. The authors also would like to acknowledge the great support from the Institute of building materials in China Academy of Building Research on the concrete material experiments to study the time-dependent thermal properties.

Conflict of interest

We declare that we have no commercial or associative interest that represents a conflict of interest in connection with the work submitted.

References

- Abbasi, A. and Hogg, P.J. (2005), "A model for predicting the properties of the constituents of a glass fibre rebar reinforced concrete beam at elevated temperatures simulating a fire test", *Compos. Part B Eng.*, **36**(5), 384-393.
- ACI 207 (2007), Report on Thermal and Volume Change Effects

- on Cracking of Mass Concrete, American Concrete Institute, Farmington Hills, MI, USA.
- ACI 231 (2010), Report on Early-Age Cracking: Causes, Measurement and Mitigation, American Concrete Institute, Farmington Hills, MI, USA.
- Amin, M.N., Kim, J.S., Lee, Y. and Kim, J.K. (2009), "Simulation of the thermal stress in mass concrete using a thermal stress measuring device", *Cement Concrete Res.*, **39**(3), 154-164.
- Asan, H. (2006), "Numerical computation of time lags and decrement factors for different building materials", *Build. Environ.*, **41**(5), 615-620.
- ASTM C 1074-11 (2011), Standard Practice for Estimating Concrete Strength by Maturity Method, American Society for Testing and Materials; West Conshohocken, PA, USA.
- Buffo-Lacarrière, L., Sellier, A., Turatsinze, A. and Escadeillas, G. (2011), "Finite element modelling of hardening concrete: application to the prediction of early age cracking for massive reinforced structures", *Mater. Struct.*, **44**, 1821-1835.
- Cai, Z.Y. (1979), *Concrete Properties*, China Architecture & Building Press, Beijing, China. (in Chinese)
- Chen, C.H. (2006), "Analysis of temperature field and thermal stress in construction considering the influence of reinforcement", Master Thesis, Hohai University, Nanjing. (in Chinese)
- Dahmani, L. (2011), "Thermomechanical response of LNG concrete tank to cryogenic temperatures", *Strength Mater.*, **43**(5), 526-531.
- De Schutter, G. (2002), "Finite element simulation of thermal cracking in massive hardening concrete elements using degree of hydration based material laws", *Comput. Struct.*, **80**, 2035-2042.
- Di Luzio, G. and Cusatis, G. (2009), "Hygro-thermo-chemical modeling of high performance concrete. I: Theory", *Cement Concrete Compos.*, **31**(5), 301-308.
- Di Luzio, G. and Cusatis, G. (2009), "Hygro-thermo-chemical modeling of high performance concrete. II: Numerical implementation, calibration, and validation", *Cement Concrete Compos.*, **31**(5), 309-324.
- GB 175-2007/XG2-2015 (2015), Common Portland cements, Standardization Administration of China, Standards Press of China, Beijing, China.
- GB 50176-2016 (2016), Code for thermal design of civil building, Ministry of Housing and Urban-Rural Development of the PRC, China Architecture & Building Press, Beijing, China.
- GB 50736-2012 (2012), Design code for heating ventilation and air conditioning of civil buildings, Ministry of Housing and Urban-Rural Development of the PRC, China Architecture & Building Press, Beijing, China.
- GB/T 10294-2008 (2008), Thermal insulation-Determination of steady-state thermal resistance and related properties-guarded hot plate apparatus, Standardization Administration of China, Standards Press of China, Beijing, China.
- GB/T 50081-2002 (2002), Standard for test method of mechanical properties on ordinary concrete, Ministry of Housing and Urban-Rural Development of the PRC, China Architecture & Building Press, Beijing, China.
- Hattel, J.H. and Thorborg, J. (2003), "A numerical model for predicting the thermomechanical conditions during hydration of early-age concrete", *Appl. Math. Model.*, **27**(1), 1-26.
- Ilc, A., Turk, G., Kavčič, F. and Trtnik, G. (2009), "New numerical procedure for the prediction of temperature development", *Automat. Constr.*, **18**(6), 849-855.
- Jendele, L., Šmilauer, V. and Červenka, J. (2014), "Multiscale hydro-thermo-mechanical model for early-age and mature concrete structures", *Adv. Eng. Softw.*, **72**(2), 134-146.
- Jeon, S.J., Jin, B.M., Kim, Y.J. and Chung, C.H. (2007), "Consistent thermal analysis procedure of LNG storage tank",

- Struct. Eng. Mech.*, **25**(4), 445-466.
- Kim, K.H., Jeon, S.E., Kim, J.K. and Yang, S. (2003), "An experimental study on thermal conductivity of concrete", *Cement Concrete Res.*, **33**(3), 363-371.
- Klemczak, B.A. (2014), "Modeling thermal-shrinkage stresses in early age massive concrete structures-comparative study of basic models", *Arch. Civil Mech. Eng.*, **14**, 721-733.
- Lee, Y., Choi, M.S., Yi, S.T. and Kim, J.K. (2009), "Experimental study on the convective heat transfer coefficient of early-age concrete", *Cement Concrete Compos.*, **31**(1), 60-71.
- Martinelli, E., Koenders, E.A.B. and Caggiano, A. (2013), "A numerical recipe for modelling hydration and heat flow in hardening concrete", *Cement Concrete Compos.*, **40**, 48-58.
- Neville A.M. (1995), *Properties of Concrete*, Longman, UK.
- Qin, F., Fan, F., Li, Z., Qian, H.L. and Jin, X.F. (2014), "Thermal simulation of hydration heat in slab of Taishan nuclear power plant unit 2", *Proceedings of the 2014 International Conference on Computing in Civil and Building Engineering*, Orlando, Florida, United States, June.
- SL 352-2006 (2006), Test Code for Hydraulic Concrete, Ministry of Water Resource of the PRC, China Water Power Press, Beijing, China.
- Wang, Q., Yan, P.Y. and Feng, J.J. (2013), "Design of high-volume fly ash concrete for a massive foundation slab", *Mag. Concr. Res.*, **65**(2), 71-81.
- Wang, X.F., Li, D.W., Han, N.X. and Xing, F. (2016), "Early age behavior analysis for reinforced concrete bridge pier", *Comput. Concrete*, **18**(5), 1041-1051.
- Zhai, X.M., Wang, Y.H. and Wang, H. (2016), "Thermal stress analysis of concrete wall of LNG tank during construction period", *Mater. Struct.*, **49**, 2393-2406.
- Zhou, Y., Meng, D. and Wang, Y.F. (2014), "Finite element simulation of hydration and creep of early-age concrete materials", *J. Mater. Civ. Eng.*, **26**(11), 05014006.
- Zhu, B.F. (2013), *Thermal Stresses and Temperature Control of Mass Concrete*, Butterworth-Heinemann, Oxford, UK.
- Zreiki, J., Bouchelaghema, F. and Chaouche, M. (2010), "Early-age behaviour of concrete in massive structures, experimentation and modelling", *Nucl. Eng. Des.*, **240**(10), 2643-2654.